Urban Climate 64 (2025) 102685

Contents lists available at ScienceDirect

Urban Climate

journal homepage: www.elsevier.com/locate/uclim

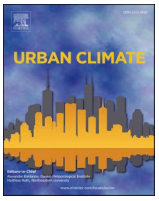

Atmospheric deposition of potentially toxic elements in a peri-urban industrial landscape: Evaluating legacy vs. current pollution

Fabrizio Monaci [a,b,*], Davide Baroni [c]

[a] Department of Life Sciences, University of Siena, Via A. Mattioli 4, Siena 53100, Italy
[b] National Biodiversity Future Center (NBFC), 90133 Palermo, Italy
[c] Department of Physical, Earth and Environmental Sciences, University of Siena, Via A. Mattioli 4, Siena 53100, Italy

ARTICLE INFO

Keywords:
Potentially toxic elements (PTEs)
Arsenic
Zinc
Manganese
Atmospheric deposition
Pyrite roasting
Peri-urban area

ABSTRACT

This study investigated the atmospheric deposition of 13 potentially toxic elements (PTEs; As, Cd, Co, Cr, Cu, Mn, Ni, Pb, Sb, Sn, Tl, V, Zn) in the historically industrialised Scarlino Plain, Tuscany (Italy). Monthly bulk deposition was monitored over one year at three strategically selected sites, revealing marked spatial and temporal variability, with Zn and Mn dominating flux profiles. Comparison with reference values suggests moderate contamination characteristics of peri-urban contexts, yet lower than levels reported for heavily industrialised areas. Multivariate analysis linked PTE deposition patterns to both geogenic and anthropogenic sources, including legacy pyrite roasting, current industrial activity and vehicular emissions. While major elements showed relatively uniform behaviour across sites, minor elements (Sb, Sn, Co, and Pb) exhibited site-specific peaks, likely reflecting episodic local anthropogenic contributions. The differences among the sites were further modulated by wet and dry deposition dynamics under local meteorological conditions. Based on the calculated soil-to-deposition (S/D) ratios, current atmospheric inputs exert minimal influence on soil PTE concentrations, which are primarily driven by historical contamination. This is particularly evident for As, Mn, and Co, where present-day deposition constitutes only a small fraction of the legacy loads. Despite declining emissions, legacy pollution continues to influence both soil and atmospheric PTE dynamics via particle resuspension, highlighting the need for targeted remediation and long-term monitoring. These findings refine our understanding of PTE cycling in peri-urban settings and support integrated management strategies in areas impacted by past and ongoing emissions.

1. Introduction

Atmospheric deposition plays a critical role in the cycling of elements within ecosystems and serves as a major pathway for the transfer of potentially toxic elements (PTEs) into terrestrial and aquatic environments (Pan and Wang, 2015). These elements derive from natural sources, including soil dust, volcanic activity, marine aerosols, and wildfires, as well as from anthropogenic activities such as industrial emissions, fossil fuel combustion, road traffic, agriculture, and biomass burning (Liu et al., 2024). Through deposition processes, PTEs are introduced or enriched in soils and surface waters, influencing their distribution, transformation, bioavailability,

* Corresponding author at: Department of Life Sciences, University of Siena, Via A. Mattioli 4, Siena 53100, Italy.
E-mail addresses: fabrizio.monaci@unisi.it (F. Monaci), davide.baroni@unisi.it (D. Baroni).

https://doi.org/10.1016/j.uclim.2025.102685
Received 6 June 2025; Received in revised form 14 October 2025; Accepted 30 October 2025
Available online 5 November 2025

and ecological toxicity (Vandeuren et al., 2023). While atmospheric deposition can supply essential micronutrients (e.g., Fe, Mo, and V) that support ecosystem productivity, excessive deposition, particularly of anthropogenic origin, often disrupts biogeochemical processes and leads to the accumulation of toxic elements, posing risks to sensitive organisms and ecological functions (Chen et al., 2022).

Atmospheric deposition occurs through two primary mechanisms: wet and dry deposition. Wet deposition predominantly affects soluble elements during precipitation events, whereas dry deposition dominates in arid and semi-arid regions, contributing substantially to total elemental fluxes (Liu et al., 2024). The interaction between local emission sources and the long-range atmospheric transport of trace-element-enriched particles creates additional complexity, resulting in significant spatial and temporal variability in deposition patterns. This heterogeneity complicates environmental impact assessments and requires site-specific monitoring strategies (Adhikari et al., 2023; Jiang et al., 2024; Ma et al., 2024).

Even low-emission industrial activities substantially contribute to the accumulation of PTEs in the surrounding soil (Pan et al., 2021). Owing to their low mobility, toxic metals and metalloids tend to persist and form contamination hotspots that often exceed regulatory thresholds (Liu et al., 2023). Atmospheric deposition is often the dominant pathway for such enrichment. For instance, in the vicinity of alumina smelting and glass manufacturing facilities, over 89 % of Cd inputs to both paddy and dryland soils have been attributed to atmospheric deposition (Yao et al., 2024). Similarly, Zn smelting operations have been shown to increase the soil concentrations of Cd, Pb, and Zn in adjacent areas (Yu et al., 2022). In addition to industrial sources, urban and traffic-related emissions play critical roles. These sources are particularly relevant in peri-urban agricultural zones, where the atmospheric deposition of Pb, Ni, and Cr from vehicular exhaust and urban activities has been identified as a major contributor to soil contamination (Liao et al., 2021; Zhang et al., 2018).

Long-term atmospheric deposition represents a major pathway delivering PTEs to soils and agricultural systems. National-scale monitoring in China revealed that atmospheric inputs contribute approximately half or more of the total inputs for As, Cd, Cr, Hg, Ni, and Pb, with Cd posing the highest potential ecological risk among the deposited metals (Ma et al., 2024). A meta-analysis of particulate matter revealed that As drives non-carcinogenic inhalation risk, whereas Cr drives carcinogenic risk. Despite marked declines in atmospheric heavy metal burdens under stricter regulatory controls, distinct spatial hotspots persist (Yu et al., 2023). Mechanistic mapping identified elevated fluxes in the high-emission regions of Eastern and Northern China via atmospheric transport and in precipitation-rich southern regions through washout processes, confirming persistent regional contamination patterns (Jiang et al., 2024). Field evidence from Hunan Province demonstrates that atmospheric deposition substantially contributes to Cd and Pb accumulation in rice grains within industrial settings, where grain-based hazard quotients can exceed safe consumption thresholds (Yu et al., 2024).

Effective management of PTE pollution necessitates sustained monitoring and stringent control of emissions from both industrial and urban sources, with targeted surveillance in regions with concentrated industrial activity being critical for identifying and mitigating localised contamination (Feng et al., 2023; Li et al., 2020). Recent advances have strengthened the empirical basis for understanding the atmospheric bulk deposition of PTEs through multi-year field studies that explicitly separate wet and dry inputs and apply receptor models, such as positive matrix factorisation (PMF), to resolve source mixtures and seasonal dynamics. For instance, in rural Beijing, PMF analysis distinguished agricultural, dust, coal combustion, industrial, and traffic contributions to bulk fluxes from 2016 to 2020 (Pan et al., 2021), while national- to regional-scale assessments across China have quantified bulk fluxes and risk metrics, revealing large spatial heterogeneity between dry- and wet-dominated regions (Pan and Wang, 2015; Ma et al., 2024; Jiang et al., 2024). Experimental evidence demonstrates that deposited metals are bioavailable and can enter crops via both root and foliar pathways, with foliar uptake of Cu, Zn, and Pb contributing substantially to grain burdens, reinforcing the need for site-resolved flux data near inhabited and agricultural areas (Xia et al., 2024).

Despite these methodological advances, the European regulatory framework remains fragmented. Although some EU Member States have established guidance values for metal deposition and Germany has linked deposition to ecosystem integrity through critical-load concepts, comprehensive monitoring of atmospheric bulk deposition remains inconsistent across the region (Ianiri et al., 2024). This monitoring gap is particularly problematic for assessing the cumulative environmental and public health impacts in industrially intensive areas.

Italy exemplifies this regulatory deficit: despite repeated calls for systematic monitoring, nationally codified reference values are absent, and recently published local-scale quantifications are limited to a few heavy industrial hubs, such as Milazzo–Priolo in Sicily (Brugnone et al., 2023; Ianiri et al., 2024). For historically contaminated Mediterranean settings with complex industrial legacies, datasets linking current atmospheric inputs to legacy soil contamination are particularly scarce (Brugnone et al., 2023), which hinders effective risk assessment and management strategies.

To address this gap, our study provides a year-long, multi-site quantification of bulk (wet + dry) deposition fluxes for a historically contaminated Tuscan industrial plain, linking atmospheric inputs to contemporaneous topsoil inventories and risk benchmarks. The Casone Industrial Area within the Scarlino Plain represents an ideal test case, with its well-documented legacy of pyrite roasting (ceased in the mid-1990s) and ongoing chemical manufacturing, allowing us to test specific hypotheses about the relative contributions of historical versus contemporary contamination sources. We hypothesised that: *i*) current atmospheric PTE deposition in the Scarlino Plain would exhibit intermediate contamination levels, exceeding remote baseline values but remaining below those of active heavy industrial zones, reflecting the transition from historical pyrite processing to modern light industry; *ii*) spatial deposition patterns would reveal distinct source signatures, with legacy-associated elements (for example As, Mn) showing uniform distribution from soil resuspension, while traffic- and industry-related elements (e.g. Sb, Pb) would display localised hotspots near contemporary sources; and *iii*) soil-to-deposition ratios would demonstrate that legacy contamination dominates current soil PTE inventories, with atmospheric inputs contributing minimally to total soil burdens, except for elements with ongoing anthropogenic emissions.

To test these hypotheses, we: *i*) quantified the bulk deposition fluxes of 13 PTEs (As, Cd, Co, Cr, Cu, Mn, Ni, Pb, Sb, Sn, Tl, V, Zn) across three strategically positioned sites over 12 months, capturing spatial gradients from industrial to peri-urban settings; *ii*) applied multivariate statistical approaches to discriminate between geogenic backgrounds, legacy industrial signatures, and contemporary anthropogenic inputs; *iii*) benchmarked fluxes against TA Luft guidelines and ecosystem-specific critical loads to assess current risk levels; and *iv*) calculated soil-to-deposition ratios using paired atmospheric and topsoil data to quantitatively partition legacy versus ongoing contributions. This integrated approach directly addresses the identified knowledge gap regarding the relative importance of historical contamination versus current emissions in post-industrial Mediterranean landscapes, with implications for risk assessment and remediation prioritisation in similar settings globally.

2. Materials and methods

2.1. Study area

The Scarlino Plain is a coastal region in southwestern Tuscany, Central Italy, encompassing an area of approximately 60 km^2 (Fig. 1). It borders the Gulf of Follonica to the west and is flanked to the northeast by the Colline Metallifere, a range of metalliferous hills rising to elevations of up to 500 m above sea level. The region is characterised by a Mediterranean climate, with a mean annual temperature of 15.9 °C and an average annual precipitation of 655 mm. Rainfall is markedly seasonal, with maxima in autumn and minima in summer. Most of the local population resides in the coastal town of Follonica (approximately 21,800 inhabitants) and in the inland settlement of Scarlino Scalo (around 1500 inhabitants), situated in the eastern portion of the plain.

Historically, the Scarlino Plain has been dominated by extensive wetland systems. Major drainage interventions began in the early 19th century, resulting in the reclamation of much of the area and leaving behind a residual freshwater basin, known as the Padule, and a network of natural and artificial watercourses. Among these, the Pecora River, originating in the Colline Metallifere, plays a key role, along with engineered channels such as the Canale Allacciante (Fig. 1). The geochemical profile of the plain is largely governed by these hydrological connections to the mineral-rich Colline Metallifere. Consequently, the alluvial deposits and surface soils in the area exhibit elevated concentrations of PTEs, including As, Cu, Fe, S, and Zn (Rossato et al., 2011). Previous studies have identified widespread anomalies in topsoil As and Zn levels, attributable to both the natural geochemical background of the region and anthropogenic inputs (Monaci and Baroni, 2025).

Within the Scarlino Plain, the Casone area has functioned as a hub of industrial activity since the mid-20th century (Fig. 1). Major operations commenced in the early 1960s with the production of sulfuric acid and iron pellets through pyrite roasting. Pyrite extracted from the Colline Metallifere was subjected to high-temperature oxidation, resulting in substantial acidic effluents, ash, and tailings. These processes have led to significant environmental impacts, including soil and water acidification and the widespread dispersal of pyritic residues, which continue to present environmental challenges. Subsequently, remediation and containment measures were

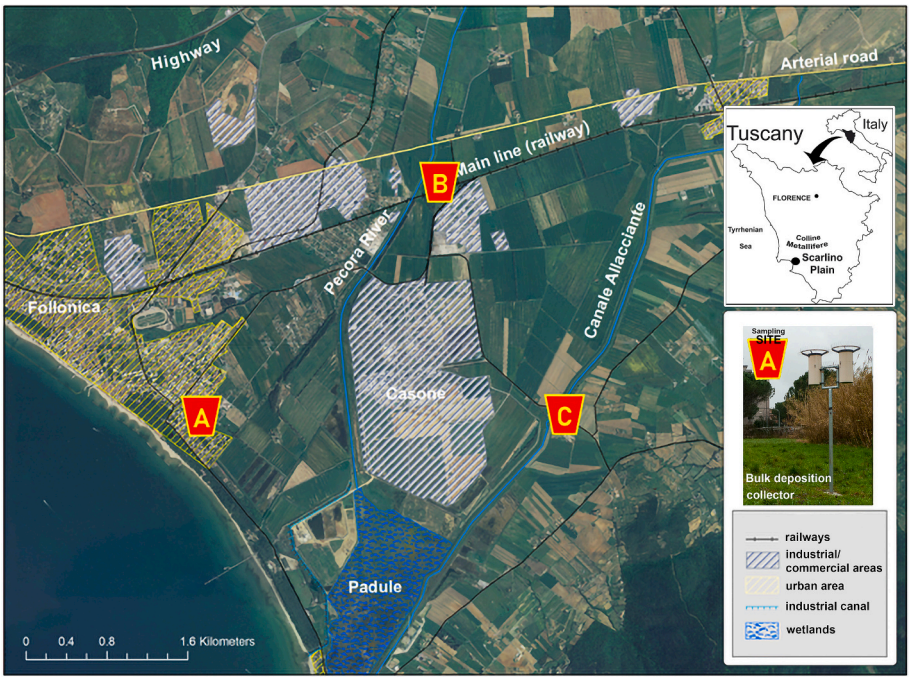

Fig. 1. Location of the study area in the Scarlino Plain (southwestern Tuscany, Italy), indicating the main land use categories derived from CORINE Land Cover data and the positions of the bulk atmospheric deposition sampling sites (A, B, and C).

implemented to mitigate soil and groundwater contamination. By the mid-1990s, industrial activities had shifted toward the chemical sector, including petroleum-based sulfuric acid production, titanium dioxide synthesis from ilmenite, and waste-to-energy incineration. The latter involved repurposing former pyrite-roasting furnaces to process non-hazardous waste and biomass for energy recovery.

2.2. Sampling of bulk atmospheric deposition

This study used a methodology to determine As, Cd, Co, Cr, Cu, Mn, Ni, Pb, Sb, Sn, Tl, V, and Zn in total atmospheric deposition (wet and dry) in compliance with EU Directive 2004/107/EC. This approach encompasses sampling using a "bottle + funnel" passive collector system, sample preparation, analysis, and quality control procedures. The method was originally applied to As, Cd, and Ni, and supports detection down to deposition fluxes of 1 ng m^{-2} d^{-1} with monthly sampling frequency. Total deposition was assessed using a bulk deposition collector designed for the atmospheric sampling of both organic and inorganic micropollutants, in accordance with the protocols established by Legislative Decree 155/10 and the guidelines outlined in the Istituto Superiore di Sanità Report 06/38 (Menichini et al., 2006).

Atmospheric deposition sampling sites were strategically selected to optimise data representativeness, with the prevailing wind direction identified as a primary criterion. Meteorological data provided by the ARPAT Provincial Department of Grosseto (ARPAT, 2011) indicated that the dominant winds in the study area originated from the NE/*E*-NE sector. This information is essential for locating sites that are most likely to intercept airborne contaminants from both industrial and natural sources. By aligning the positioning of the sampling stations with dominant wind trajectories, this study aimed to reliably capture deposition patterns in accordance with established best practices in the literature (Fernández-Olmo et al., 2015).

To ensure data integrity and minimise external interference, the siting of the collection stations was carefully considered. The following criteria guided their placement:

- Avoidance of physical obstruction. The stations were positioned to prevent interference from buildings, vegetation, or other structures that could impede particulate deposition or alter local airflow patterns.
- Distance from emission sources. To reduce the risk of contamination from localised emissions, stations were located at an appropriate distance from industrial stacks, major roadways, and other identifiable point sources.
- Security and accessibility. Sites were selected to minimise the risk of tampering, accidental disruption, or vandalism while ensuring ease of access for regular maintenance and sample retrieval.
- Environmental representativeness. Sampling sites were distributed to capture the heterogeneity of the Scarlino Plain and adjacent areas, considering land use, topography, and proximity to the Gulf of Follonica to reflect a broad spectrum of depositional inputs.
- Compliance with standard protocols. The deployment and operation of bulk deposition samplers followed established guidelines for atmospheric deposition monitoring, ensuring a consistent sampler design, suitable installation height, and standardised collection intervals to enable robust inter-site comparisons.

A cylindrical bulk deposition sampler was used, consisting of a 10-L high-density polyethylene (HDPE) bottle fitted with a 25 cm diameter cylindrical funnel. The height-to-diameter ratio of the funnel exceeded 1:1, promoting the efficient collection of both wet and dry atmospheric deposits. To prevent contamination, all the components were constructed entirely from plastic materials. The sampler was housed within an opaque, light-coloured plastic shielding tube designed with an air gap to minimise thermal transfer and protect samples from light exposure. The upper edge of the shield was aligned with the funnel rim, and an external deterrent ring was installed to prevent birds and other animals from perching (Fig. 1, inset; Fig. S1, Supplementary Material). Samplers were mounted at heights exceeding 3 m in open, unobstructed locations to ensure representative deposition capture, free from interference from nearby structures.

A monitoring network for atmospheric deposition using passive bulk collectors was established in January 2014. Three collection stations (Stations A, B, and C) were deployed within the study area surrounding the Casone industrial complex (Fig. 1). Monitoring commenced in February 2014 and continued for 12 months (Table S1, Supplementary Material). Samples were collected at regular intervals of 30 ± 2 days, in accordance with the methodology outlined by Menichini et al. (2006).

At the sampling site, the protective coverings of the bottle and funnel were removed prior to exposure. Following the sampling period, the funnel and bottle were separated and sealed with a PTFE-gasketed cap. To prevent photodegradation and contamination, the components were transported to the laboratory in sealed, light-protected containers (Fig. S1). Upon arrival at the laboratory, the samples were visually inspected to remove any foreign material, such as insects or plant debris, using PTFE-tipped tweezers. The inner surface of the funnel was then rinsed with 100 mL of 2 % nitric acid (HNO_3), followed by ultrapure water, and these rinses were combined with the contents of the collection bottles. In the absence of wet deposition, 200 mL of ultrapure water was added to the bottle, which was then shaken to suspend the deposited particles adhering to the inner surface. All samples were filtered under vacuum using 0.45 μm cellulose acetate filters. The filtrate was collected in acid-cleaned flasks, and the retained particulates on the filter were inspected for residual debris, which was removed and rinsed with ultrapure water. To maximise sample recovery, both the collection bottle and filtration apparatus were thoroughly rinsed with ultrapure water.

2.3. Chemical treatment and PTEs analysis

Particulate matter retained on the filters was digested using a microwave-assisted digestion system equipped with PTFE vessels and quartz inserts. Each filter was treated with 1 mL of concentrated HNO_3 and placed in a PTFE container preloaded with 5 mL of 5 %

hydrogen peroxide (H_2O_2). This protocol ensured efficient mineralisation while minimising the formation of nitrogen oxide fumes and the potential loss of analytes. To stabilise the filtrate, concentrated HNO_3 was added directly to the solution. For samples with large volumes, aliquots were gently concentrated at temperatures below 60 °C in PTFE beakers under a fume hood to enhance the analytical sensitivity. The prepared samples were analysed for selected potentially toxic elements (PTEs) using Inductively Coupled Plasma Mass Spectrometry (ICP-MS) in accordance with the UNI EN 14902 standard (UNI, 2005a). High-purity reagents and contamination-verified materials were employed throughout the procedure to minimise analytical interference from trace metal impurities.

All analyses were conducted by an ACCREDIA-accredited commercial testing laboratory in accordance with UNI CEI EN ISO/IEC 17025:2005 (UNI, 2005b), the standard in effect at the time of analysis, ensuring data reliability through standardised protocols. The comprehensive QA/QC program included systematic blank controls, certified reference material validation and duplicate analyses. Process blanks were prepared by rinsing clean HDPE bottles with 500 mL of ultrapure water, which was allowed to flow along the inner surface of the sampling funnels to replicate field exposure conditions. These blanks, along with method blanks for each analytical batch, were subjected to the same digestion and analytical protocols as the samples to account for any contamination from materials, reagents, or procedural handling.

Analytical accuracy and precision were verified using certified reference materials (CRMs) from the National Institute of Standards and Technology (NIST, Gaithersburg, MD, USA). NIST SRM 1648a (Urban Particulate Matter) served as the primary reference material, providing certified values for all 13 PTEs. Method validation across different matrices was ensured through the analysis of NIST SRM 1643f (Trace Elements in Water) for aqueous filtrates and NIST SRM 2710a (Montana I Soil) for particulate matter. CRMs underwent identical microwave-assisted digestion procedures as samples and were analysed every 10 samples to monitor instrumental drift and ensure consistent performance throughout the analytical sequence. Duplicate analyses were performed for every batch, achieving recoveries of 92–107 % of the certified values (mean: 98.5 ± 4.2 %) with relative standard deviations below 5 % for replicate analyses ($n = 3$). These performance metrics, maintained in accordance with the UNI EN 14902 standard requirements, confirmed the reliability of the digestion protocol and ICP-MS quantification procedures.

The deposition flux (μg m^{-2} d^{-1}) of each metal was calculated using the following equation:

$$Flux = \frac{C \bullet V}{A \cdot t}$$

The total deposition flux was calculated as the sum of the fluxes from both the filter-retained and filtrate fractions, where C is the metal concentration (μg mL^{-1}), V is the sample volume (mL), A is the funnel area (m^2), and t is the collection period (days). This approach accounts for the complete contribution of the deposited material collected in both phases.

All analytical procedures were conducted in accordance with strict safety protocols because of the hazardous nature of the reagents employed. Comprehensive documentation was maintained throughout the sampling and analytical workflow, including georeferenced site locations, environmental conditions during sampling, and deviations from standard operating procedures.

2.4. Statistical analysis

Statistical analysis was performed to characterise the variability of PTE deposition fluxes across the three sampling sites and assess the influence of environmental conditions on deposition patterns. Prior to the main analyses, data normality was evaluated using the Kolmogorov-Smirnov and Lilliefors tests, and Levene's test was applied to verify homogeneity of variances. The coefficient of variation (CV) was calculated to highlight the inter-site differences in elemental variability and deposition trends.

To reduce dataset dimensionality and identify patterns in PTE deposition, Principal Component Analysis (PCA) was conducted on the centred log-ratio clr-transformed data. The clr transformation, applied using CoDaPack 2.0 (Comas-Cufí and Thió-Henestrosa, 2011), accounted for the compositional nature of the dataset and addressed the constraints associated with the closed data. Principal components (PCs) with eigenvalues greater than 1 were retained based on the Kaiser criterion. Each PC was interpreted using its loading scores and explained variance to identify the elements contributing most significantly to the overall variability.

K-means clustering was applied to the PCA-transformed dataset to classify the observations into groups with similar deposition profiles. This multivariate approach facilitated further dimensionality reduction and enabled the association of compositional patterns with potential environmental and anthropogenic drivers. The optimal number of clusters was identified using the elbow method, and cluster validity was assessed by visually inspecting their distribution within the PCA space.

To assess whether rainfall varied significantly across the identified clusters, an Analysis of Variance (ANOVA) was performed. When significant differences were detected, Tukey's Honest Significant Difference (HSD) test was used for post-hoc comparisons to determine which clusters exhibited distinct rainfall regimes.

All statistical analyses were conducted using R version 4.5.0 (R Core Team, 2025), the FactoMineR package for PCA (Lê et al., 2008), ggplot2 for visualisation (Wickham, 2016), and dplyr for data manipulation (Wickham et al., 2023).

3. Results and discussion

3.1. PTE fluxes in atmospheric bulk deposition

To characterise the deposition patterns of potentially toxic elements (PTEs) in the vicinity of the Casone industrial complex, monthly bulk deposition samples were collected over one year from three strategically selected sites. Table 1 reports the descriptive statistics for the monitored metals and metalloids, along with reference threshold values for As, Cd, Ni, Pb, and Tl, derived from

Germany's TA Luft (2002) guidelines. These threshold values refer to immission limits (i.e. ambient concentrations of pollutants at receptor surfaces) and are not ecologically derived critical loads. Instead, they represent enforceable administrative standards established under the German air quality legislation. In the absence of specific national or European regulatory standards, these thresholds have been formally adopted by the Regional Environmental Protection Agency of Tuscany (ARPAT, 2014) and other local institutions as reference values for regional atmospheric monitoring programs.

Beyond these operational benchmarks, we incorporated ecosystem-specific critical load values from Schlutow et al. (2021): CL$(M)_{eco}$, CL$(M)_{drink}$, and CL$(M)_{food}$, which protect ecosystem integrity, groundwater quality for human consumption, and food safety through wheat grain exposure, respectively. These thresholds were derived from steady-state mass balance calculations following the CLRTAP guidelines, balancing long-term atmospheric inputs against outputs (crop removal, leaching) to avoid exceeding ecotoxicologically relevant no-effect concentrations or WHO standards.

Critical loads are site-specific and depend on the soil pH, organic matter content, percolation rates, and crop yields. Schlutow et al. acknowledged that their German-derived values, based on acidic soils and moderate biomass production, have limited transferability to other environments. Mediterranean soils in the Scarlino Plain are typically more alkaline, less leaching-prone, and more intensively cultivated, potentially supporting higher critical loads than those predicted by the German models. Nevertheless, these values provide a useful comparative framework for preliminary risk assessment in the absence of Italy specific thresholds.

Comparing measured PTE fluxes against TA Luft limits, critical loads, and literature values (Table 1; Supplementary Table S3) creates a robust multi-criteria assessment framework for ecological risks from atmospheric deposition. This approach highlights the need for harmonised regulatory standards at the national and EU levels while contextualising local patterns within broader regional transport dynamics (Guo et al., 2017; Pan et al., 2021).

Monthly bulk deposition fluxes of As, Cd, Co, Cr, Cu, Mn, Ni, Pb, Sb, Sn, Tl, V, and Zn varied substantially, spanning nearly two orders of magnitude, from as low as 0.05 μg m^{-2} d^{-1} for Cd to approximately 30 μg m^{-2} d^{-1} for Zn. Certain elements, notably Sn, exhibited high variability, with coefficients of variation (CV%) of up to 96 %. This pronounced variability likely reflects the heterogeneity of emission sources and localised depositional inputs across the study area. Despite the observed variability, most mean fluxes remained below the limits established by the German TA Luft guidelines (TA Luft, 2002) and within or below the lower bounds of the critical load thresholds proposed by Schlutow et al. (2021) for ecosystems, drinking water, and food safety.

Compared to heavily industrialised areas such as Milazzo-Priolo Gargallo in Sicily (Brugnone et al., 2023) or Northern China (Pan and Wang, 2015), fluxes in the Scarlino Plain were generally two to three times lower, or even an order of magnitude lower in some cases, indicative of a moderately industrialised peri-urban setting rather than a high-intensity industrial source. This interpretation is further supported by a comparison with regional benchmarks: fluxes in the Scarlino Plain are substantially elevated relative to those recorded in the unimpacted Cavriglia Park, yet comparable to those observed in Badia al Pino, a similarly industrialised peri-urban area of Tuscany (ARPAT, 2014). Together, these comparisons reinforce the view that Scarlino exhibits a characteristic depositional imprint of diffuse industrial and urban emissions but not the elevated burden typical of heavily contaminated zones. Among the studied elements, As requires particular attention because of its toxicity and potential for both local and long-range transport. The Scarlino Plain, with a well-documented As-enrichment history (Costagliola et al., 2010; Rossato et al., 2011), exhibits elevated atmospheric As deposition relative to remote areas (Table 1). The mean As flux recorded (0.60 μg m^{-2} d^{-1}) remained approximately sevenfold below the TA Luft regulatory threshold of 4 μg m^{-2} d^{-1}, indicating a modest anthropogenic contribution to total atmospheric loading. Regional comparison shows that this flux is approximately twice that of the undisturbed reference site at Cavriglia Park, yet only marginally higher than other industrialised peri-urban locations in Tuscany (e.g. Badia al Pino; Table 1), suggesting a moderate anthropogenic contribution consistent with established regional industrial deposition patterns.

Table 1 contextualises the As flux data across various environments.

- Industrial sites: heavily industrialised locations show elevated fluxes, with Milazzo–Priolo Gargallo (Sicily) recording 1.0–2.5 μg m^{-2} d^{-1} (Brugnone et al., 2023), while coal-dominated regions in Northern China often exceed 6.0 μg m^{-2} d^{-1} (Pan and Wang, 2015).
- Rural and remote locations: lower fluxes characterise rural Beijing (~0.30–0.40 μg m^{-2} d^{-1}; Pan et al., 2021) and the Central Pyrenees (<0.1–0.5 μg m^{-2} d^{-1}; Camarero et al., 2017), driven primarily by long-range transport. The Scarlino Plain aligns with the upper end of this range.
- Global peri-urban contexts: Jilin Province (northeast China) shows As fluxes of 0.5 to 1.2 μg m^{-2} d^{-1} near agricultural and urban sites (Liu et al., 2024), partially overlapping the Scarlino Plain observations.

These comparisons indicate that the Scarlino Plain experiences moderate anthropogenic As influences typical of industrialised peri-urban areas. Contributions likely originated from nearby light industrial activities, augmented by residual local influences from historical arsenopyrite smelting. Additionally, given the coastal location of the study area, marine aerosols may represent a supplementary source of As deposition, although likely of lesser magnitude compared to geogenic and anthropogenic inputs (Savage et al., 2019). Although As levels appear relatively low, they represent elevated deposition in inhabited and agriculturally significant regions.

Beyond As, the fluxes of Cd, Ni, Pb, and Tl observed in this study were well below the TA Luft (2002) guidelines. For Cd, Ni, and Pb, fluxes were at or below the lower bounds of the critical loads proposed by Schlutow et al. (2021), while no critical load threshold has been established for Tl in this framework. For example, measured fluxes of 0.05 μg m^{-2} d^{-1} of Cd, 2.8 μg m^{-2} d^{-1} of Pb, and 1.8 μg m^{-2} d^{-1} of Ni, are consistent with those reported in rural-to-peri-urban areas of Tuscany (ARPAT, 2014), Northern Spain (Fernández-Olmo et al., 2015), rural Beijing (Pan et al., 2021), and the Pyrenees (Camarero et al., 2017), suggesting similar deposition patterns in moderately impacted regions.

Table 1
Descriptive statistics of monthly bulk deposition fluxes (μg m^{-2} d^{-1}) recorded over a one-year period (10 February 2014–10 February 2015; mean interval 30.4 ± 0.79 days) at three peri-urban sites near the Casone industrial area. Data are compared with the German guidelines[1] (Ta Luft, 2002) and the critical loads[2] identified by Schlutow et al. (2021) for ecosystem protection ($CL(M)_{eco}$), drinking water ($CL(M)_{drink}$), and food safety ($CL(M)_{food}$ for wheat). Reference data are also included from: Cavriglia Park and industrial sites in Tuscany[3] (ARPAT, 2014); industrial and coastal urban areas in Sicily[4] (Brugnone et al., 2023); urban, industrial, and rural environments of Northern Spain[5] (Fernández-Olmo et al., 2015); high-altitude, remote areas of the Central Pyrenees, Spain[6] (Camarero et al., 2017); industrial, urban, and agricultural sites of Northern China[7] (Pan and Wang, 2015); peri-urban and agricultural zones in Jilin Province, China[8] (Liu et al., 2024); and high-elevation sites influenced by regional transport in Southwest China[9] (Nie et al., 2017).

		As	Cd	Co	Cr	Cu	Mn	Ni	Pb	Sb	Sn	Tl	V	Zn
This study	mean	0.60	0.05	0.27	3.07	6.56	14.7	1.84	2.78	0.26	0.19	0.02	2.98	30.2
	Std. Dev.	0.32	0.03	0.22	1.68	3.39	8.03	1.12	1.19	0.21	0.19	0.01	1.80	23.0
	CV%	53.4	55.0	78.8	54.7	51.8	54.5	60.9	42.6	79.0	96.2	47.2	60.3	76.0
	median	0.55	0.04	0.20	2.94	5.84	13.9	1.67	2.87	0.17	0.13	0.02	2.47	24.4
	min	0.07	<DL	0.01	0.19	0.43	1.37	0.11	0.44	0.03	0.01	<DL	0.19	4.37
	max	1.36	0.11	0.78	8.04	15	31.0	5.17	5.25	0.73	0.69	0.03	6.71	101
	n (>DL)	36	35	36	36	36	36	36	36	36	36	24	36	36
Guidelines/	TA-Luft[1]	4	2	–	–	–	–	15	100	–	–	2	–	–
Critical loads	CL(*M*)eco[2]	4.11–457	0.41–35.0	–	21.4–287	133–7543	–	10.1–3077	0.55–713	–	–	–	–	22.2–673
	CL(*M*)drink[2]	0.60–1.64	0.68–1.92	–	3.29–189	1.92–927	–	–	0.82–38.9	–	–	–	–	338–18,941
	CL(*M*)food[2]	–	0.52–5.26	–	–	–	–	–	–	–	–	–	–	–
Geographic comparisons	Cavriglia Park, Tuscany[3]	0.3	0.04	0.1	2.3	1.6	9	0.5	0.4	0.1	0.5	0.07	0.7	22
	Badia al Pino, Tuscany[3]	0.5	0.2	0.5	2.8	15.1	38	2.3	5.5	0.2	0.8	0.01	1.4	85
	Milazzo-Priolo, Sicily[4]	1.0–2.5	0.1–0.3	0.3–0.5	10–25	10–25	25–60	5–20	25–40	0.6–1.5	–	0.03–0.1	3–10	80–150
	Northern Spain[5]	<0.5	<0.05	0.2–0.4	5–15	8–15	15–40	3–10	10–20	0.3–0.8	–	0.02–0.05	2–5	40–90
	Central Pyrenees, Spain[6]	<0.5	<0.03	<0.1	<1	<2	<5	<1	0.5–5	<0.1	–	<0.01	<1	<10
	Northern China[7]	6–8	0.8–1.0	0.8–1.0	30–40	20–30	80–120	30–50	12–15	1.0–2.5	–	0.5–1.0	8–15	200–300
	Jilin Province, China[8]	0.2–0.4	<0.1	0.2–0.4	1–3	1–3	10–20	1–3	1.2–2.0	0.2–0.4	–	0.02–0.04	1–2	20–40
	Southwest China[9]	0.1–0.3	<0.05	<0.1	2–5	2–5	5–15	1–3	<2	<0.2	–	<0.02	1–3	15–35

The mean fluxes of Co, Cr, Cu, Mn, Sb, and Zn in the study area consistently exceeded the values reported for remote locations (ARPAT, 2014; Camarero et al., 2017), suggesting local anthropogenic contributions from light industry, vehicular emissions, and agriculture. Nevertheless, these fluxes remained substantially below the levels observed in heavily industrialised areas, such as those in Sicily (Brugnone et al., 2023) and Northern China (Liu et al., 2024; Pan and Wang, 2015), reinforcing the classification of the Scarlino Plain as having a moderate peri-urban signature.

The history of mining and pyrite-smelting activities in the Scarlino region has contributed to elevated Cu levels in topsoils, reaching up to 132 μg g^{-1} (mean = 35.1 μg g^{-1}; Monaci and Baroni, 2025), compared to the European baseline of 17 μg g^{-1}. Similarly, Zn concentrations averaged 108 μg g^{-1}, with some sites exceeding 150 μg g^{-1}, reflecting diffuse industrial or urban influences on naturally elevated background levels. These conditions likely explain the moderate Cu and Zn fluxes (~7 and ~ 30 μg m^{-2} d^{-1}, respectively), which appear to result from a combination of ongoing anthropogenic emissions and the resuspension of Cu-Zn-rich dust (Batonneau et al., 2004).

A similar pattern was observed for Mn, with local soil concentrations ranging from 14.8 to 5581 μg g^{-1} (Monaci and Baroni, 2025), exceeding the European reference levels by approximately 33 % (Salminen et al., 2005). This Mn enrichment is likely influenced by sulfuric-acid-based ilmenite processing associated with TiO_2 production (Jabłoński and Tylutka, 2016). Consequently, atmospheric Mn deposition in the Scarlino Plain likely results from the wind-driven mobilisation of Mn-enriched particulates from contaminated soils, coupled with additional anthropogenic emissions. Although the measured Mn fluxes fall within the lower range of literature values (Table 1), the data point to a sustained biogeochemical enrichment dynamic, whereby both primary and secondary sources periodically elevate atmospheric Mn levels above regional background concentrations.

3.2. *Spatial and temporal variability of PTE fluxes in atmospheric bulk deposition*

Fig. 2 summarises the PTE deposition at Sites A, B, and C over the 365-day sampling period. Panel (a) ranks individual PTEs by total flux at each site, with Zn showing the highest deposition (~10,000 μg m^{-2}) and Tl the lowest (1,5 μg m^{-2}). Panel (b) illustrates the relative contributions of each PTE to the total deposition at each site using stacked bar charts, highlighting the compositional differences among the sites.

Zinc and Mn consistently dominated deposition at all sites, with Zn fluxes exceeding 12,700 μg m^{-2} at Site B and Mn ranging between 4300 and 6000 μg m^{-2}. These high fluxes are largely attributable to anthropogenic sources, including mechanical abrasion from vehicle components (e.g. tire and brake wear), manufacturing processes, and light industrial emissions, in addition to natural crustal inputs (Brugnone et al., 2023; Liu et al., 2024; Schlutow et al., 2021). Comparable Zn—Mn dominance has been reported for a coastal urban setting in Northern Spain, where PMF attributed ~62.5 % of the soluble metal flux to an industrial factor characterised by Zn and Mn. Notably, Zn showed the highest water solubility (~78 %), which helps explain its strong precipitation-modulated behaviour in bulk deposition (Fernández-Olmo et al., 2014).

Copper, Cr, and Pb also exhibited substantial variability, with site-specific fluxes ranging between 1000 and 2700 μg m^{-2}. In

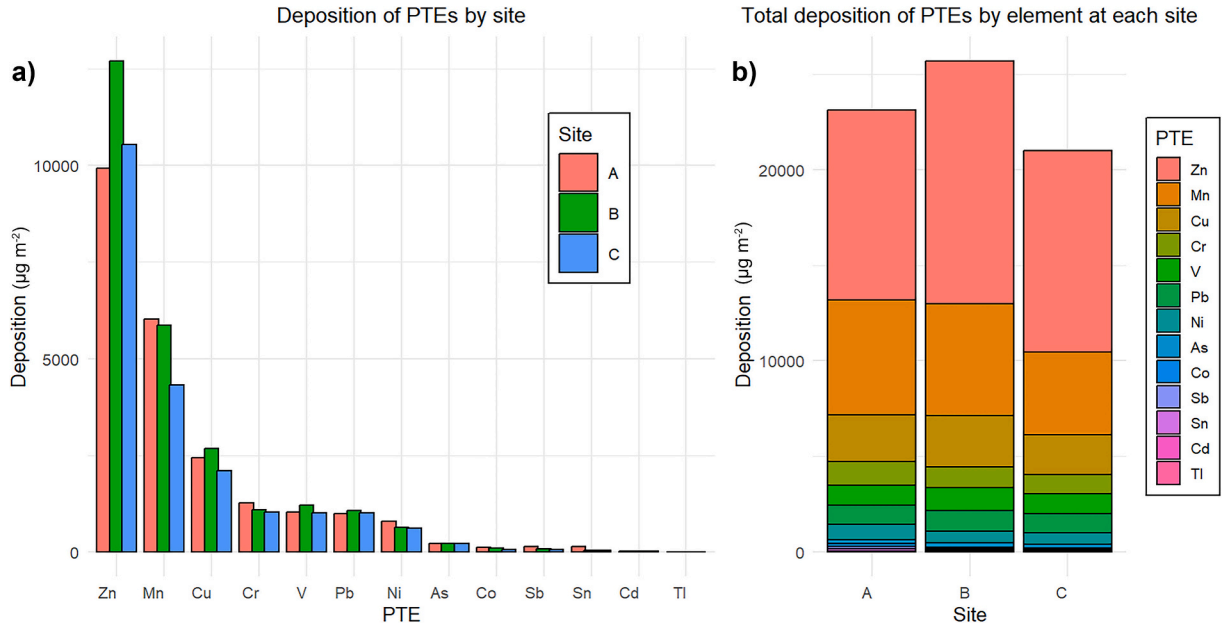

Fig. 2. PTE deposition (μg m^{-2}) across Sites A, B, and C over the 365-day sampling period. Panel (a) shows the individual PTEs fluxes by site, ranked from highest (Zn) to lowest (Tl) total deposition. Panel (b) presents the total PTE deposition at each site, shown as stacked bars indicating the relative contributions of each element.

contrast, Tl, Cd, Sn, and other minor elements exhibited significantly lower fluxes, typically below 100 μg m^{-2}. Thallium remained low across all three sites, with fluxes below 7 μg m^{-2}, while Sn ranged from 35 to 38 μg m^{-2}, and Sb ranged from 65 to 74 μg m^{-2} at Sites B and C. However, Site A was a notable exception for both Sn and Sb, recording significantly higher fluxes of 144 and 131 μg m^{-2}, respectively. Site B showed slightly elevated Zn and Mn fluxes relative to other locations. Although the relative ranking of elemental deposition was broadly consistent across the three sites, total deposition followed the order B > A > C, likely reflecting differences in proximity to the emission sources and atmospheric transport dynamics.

Site B, located near the centre of the historic industrial district, lies adjacent to the "GR66" brownfield, an area designated for remediation under the regional "Plan for the Remediation of Polluted Areas" due to extensive pyrite ash contamination. The site is also situated within the northern sector of the study area, which is characterised by intensive agricultural land use patterns. These factors likely contributed to the elevated PTE deposition at Site B, reflecting the combined influence of legacy industrial contamination and agriculture-related dust emissions.

The monthly PTE deposition trends across the three sampling sites are presented in Figs. 3 and 4. Throughout the sampling period, the deposition fluxes of As, Cd, Ni, Pb, and Tl remained consistently below the TA Luft (2002) guideline limits. Arsenic deposition exhibited limited spatial variability among sites (CV < 0.7) and moderate temporal fluctuations, with distinct peaks during the warm (June) and cold (December) seasons. These seasonal patterns likely reflect the combined influence of anthropogenic emissions and the meteorological conditions.

Fig. 5 shows a positive relationship between As deposition fluxes and monthly rainfall, although statistical significance ($p < 0.05$) was observed only at Site A. The June peak at Site C (Fig. 3) may reflect enhanced atmospheric turbulence during dry conditions, whereas the December peak across all sites likely results from wet deposition and meteorological conditions that reduce atmospheric dispersion. This relationship underscores the key role of wet deposition in transferring water-soluble elements such as As from the atmosphere to terrestrial ecosystems, consistent with previous studies (Fernández-Olmo et al., 2015; Pan and Wang, 2015). Seasonal precipitation variations modulate As fluxes over longer timescales, with higher deposition rates during wet periods than during dry periods (Ma et al., 2024; Pan et al., 2021).

In contrast to this precipitation-dependent behaviour, Sb, Sn, Pb, and Co exhibited pronounced spatiotemporal variability (Fig. 4, red shading) with minimal correlation to rainfall intensity (Fig. 5; Fig. S2, Supplementary Material). Each element showed distinct seasonal patterns: Sb and Sn fluctuated year-round, Co peaked in early summer (May–July), and Pb concentrated during the driest months (May and December). These patterns reflect the interactions between specific emission sources and atmospheric transport mechanisms.

The persistent variability of Sb and Sn indicates continuous emissions from industrial processes and traffic-related abrasion, consistent with their anthropogenic origin. Antimony, recognised as a traffic-related element, originates primarily from brake linings, where Sb_2S_3 improves friction stability (Fujiwara et al., 2011). Urban road dust studies have confirmed Sb enrichment in the finest particle fractions, correlating with Cu and Pb, with atmospheric levels 100–200 times higher from anthropogenic versus natural sources (Amato et al., 2011; Fujiwara et al., 2011). Recent investigations have demonstrated that Sb and Sn are released through

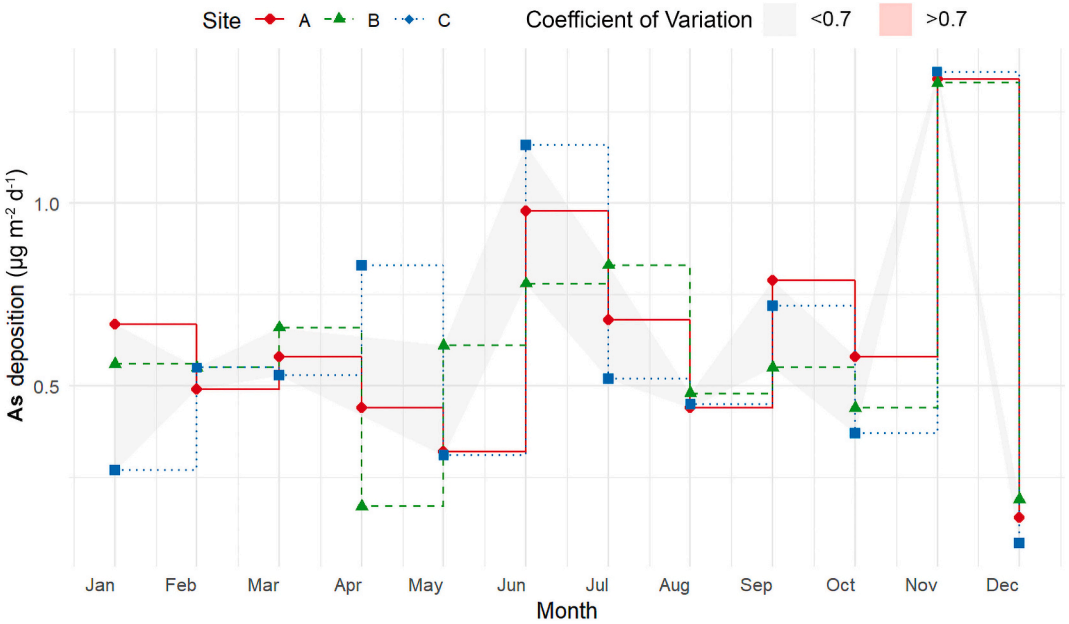

Fig. 3. Monthly As deposition fluxes (μg m^{-2} d^{-1}) at Sites A–C over the 12-month sampling period. Shaded ribbons indicate within-month variability summarized by the coefficient of variation (CV): grey denotes moderate variability (CV ≤ 0.7). High variability (CV > 0.7) was not observed at these sites; this category is retained in the legend for consistency with the study's classification scheme.

Fig. 4. Monthly trends of PTEs deposition fluxes (µg m^{-2} d^{-1}) across three sampling sites (A, B, and C) over a 12-month period. Each panel corresponds to a specific element, with site-specific measurements depicted by distinct markers (circles, triangles, and squares) and step-line profiles. Shaded areas indicate inter-site variability: red for high variability (CV > 0.7) and grey for moderate variability (CV ≤ 0.7), based on the coefficient of variation. (For interpretation of the references to colour in this figure legend, the reader is referred to the web version of this article.)

vehicle wear and submicron road dust resuspension, serving as tracers of continuous urban traffic emissions (Vlasov et al., 2025). These metals accumulate in soils through bulk deposition, contributing to terrestrial contamination and raising concerns regarding ecological and human exposure (Guo et al., 2017; Nie et al., 2017; Pan and Wang, 2015). Consistent monitoring of Sb and Sn fluxes is essential, as their atmospheric persistence implies that even moderate fluxes may pose cumulative risks to ecosystems and food security (Brugnone et al., 2023; Ianiri et al., 2024).

In contrast, the Co peak during early summer likely reflects seasonal atmospheric conditions, including enhanced photochemical activity and altered boundary layer dynamics, which promote aerosol formation and subsequent deposition. Similar seasonal patterns have been observed for other trace metals, where stronger solar radiation and a shallower boundary layer enhance secondary aerosol production and increase the particle residence time in the lower atmosphere (Camarero et al., 2017; Pan and Wang, 2015). These processes can amplify metal deposition fluxes, even in regions without direct emission changes, underscoring the importance of meteorological drivers in modulating the temporal variability of atmospheric deposition (Nie et al., 2017). This meteorological influence is particularly evident for Pb (Fig. 4), where deposition during dry periods is dominated by the dry deposition and resuspension of legacy-contaminated particles in the absence of wet scavenging. These episodic patterns likely reflect intermittent sources, such as biomass burning, agricultural activity, and industrial discharges (Pan et al., 2021; Yu et al., 2022). Sharp Sb and Sn peaks at Site A further support the role of localised point sources, possibly linked to nearby industrial installations or high traffic zones.

Fig. 6 illustrates a strong positive correlation between Sb and Sn at Site A, in contrast to the weaker correlations observed at Sites B and C. This robust relationship indicates the presence of a localised co-emitting source at Site A, which is likely associated with traffic, waste incineration, and/or industrial processes involving Sb- and Sn-containing materials. Such activities include the combustion of flame-retardant-treated plastics and the use of solder alloys and brake linings in vehicular traffic (Månsson et al., 2009; Yang et al., 2022). Site A was uniquely positioned in an urban setting adjacent to a heavily trafficked coastal road, making it particularly susceptible to traffic-related contamination. Beyond direct brake wear emissions, the resuspension of previously deposited particles from vehicular movement likely contributed to the elevated Sb and Sn concentrations observed at this site. Located downwind of the Casone industrial complex, Site A was well-suited for capturing emissions from industrial operations and urban waste treatment. In contrast, the absence of comparable signals at Sites B and C reflects their reduced exposure to industrial and urban sources, likely because of the

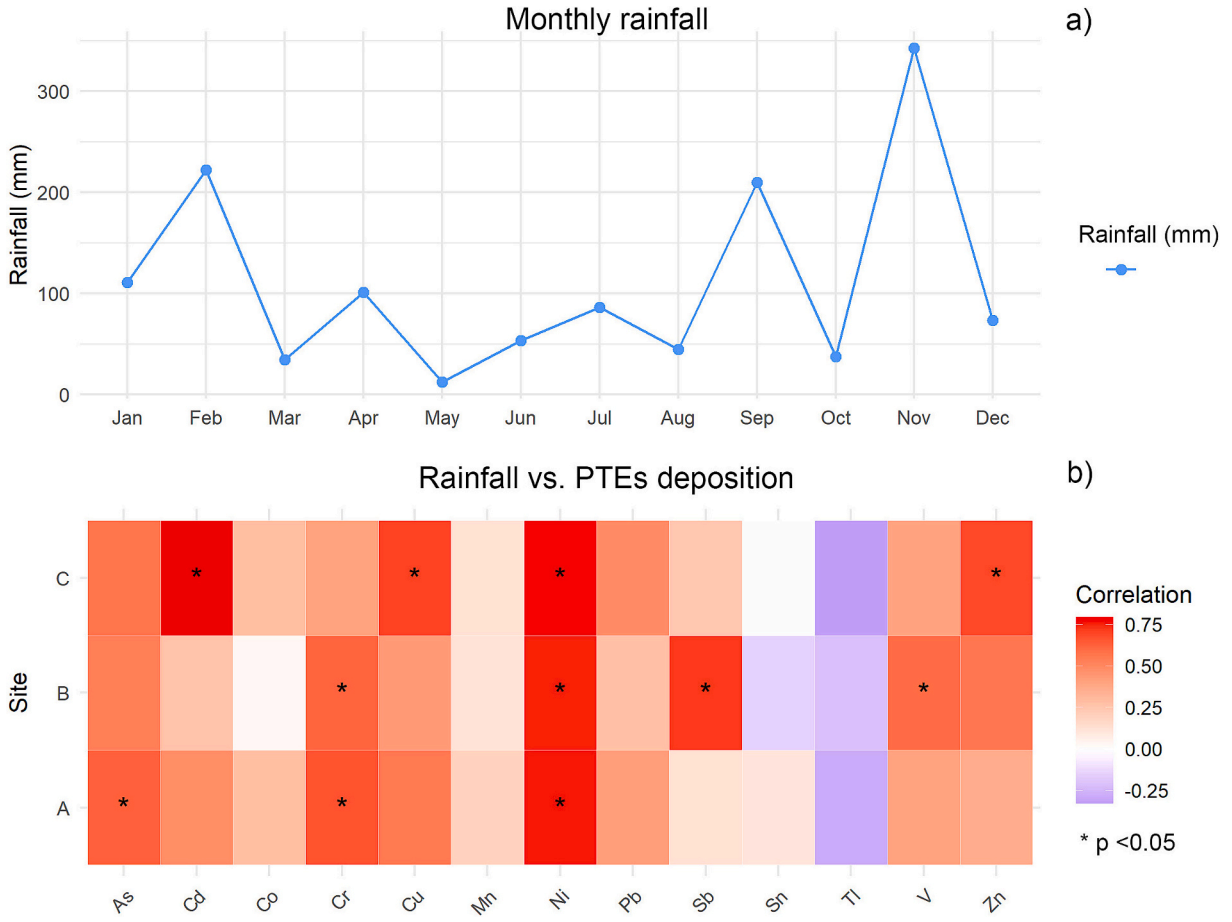

Fig. 5. (a) Monthly precipitation (mm) from January to December. (b) Heatmap showing the Pearson correlation coefficients between metal concentrations (As, Cd, Co, Cr, Cu, Mn, Ni, Pb, Sb, Sn, Tl, V, Zn) and sampling sites (A, B, and C). Warmer colours (reds) indicate stronger positive correlations, while cooler colours (purples) represent negative correlations. Asterisks (*) denote statistically significant correlations ($p < 0.05$).

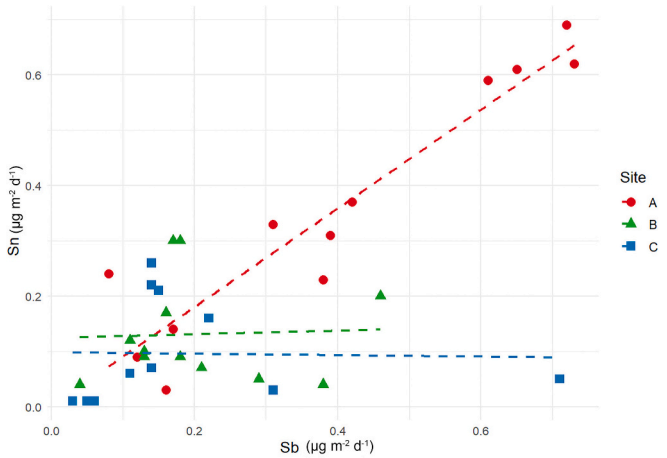

Fig. 6. Relationship between Sb and Sn deposition fluxes at the three sampling sites (A, B, and C). Data points are distinguished by colour and shape. Dashed regression lines represent site-specific trends, highlighting differences in the strength and direction of the Sb—Sn correlation across sites.

greater distance from the emission areas and different prevailing wind patterns.

While major elements like Zn and Mn dominate overall deposition flux with relatively consistent behaviour across all sites, the marked spatial variability of minor elements (Sb, Sn, and Pb) underscores the importance of localised anthropogenic inputs. These findings emphasise the value of spatially resolved, temporally continuous monitoring for identifying and characterising site-specific pollution sources in the watershed. The observed patterns reflect the complex interactions among meteorological conditions, seasonal dynamics, and anthropogenic activities that collectively govern PTE deposition across the Scarlino Plain. Consistent with this interpretation, coastal bulk deposition records from the Venice Lagoon document element-specific precipitation responses, revealing distinct coastal source fingerprints: traffic-related Cu–Zn–Pb–Sb versus ship/oil-related V—Ni. Inorganic pollutants exhibit heterogeneous rain dependence and marked inter-site contrasts, features that closely mirror our observations (Morabito et al., 2014).

3.3. *Multivariate analysis and source of PTEs in atmospheric bulk deposition*

Principal Component Analysis (PCA) was performed on the clr-transformed dataset of PTEs in bulk deposition to identify the dominant multi-element depositional patterns in the Scarlino Plain. Five principal components (PCs) with eigenvalues greater than 1 were extracted, collectively explaining 78.4 % of the total variance in the data.

PC1 (23.3 % of variance) exhibited strong positive loadings for Cr (0.69) and Ni (0.76), indicating a geogenic origin linked to natural soil composition (Monaci and Baroni, 2025). In the Colline Metallifere, locally occurring ophiolitic slices (mafic–ultramafic lithologies) are documented and naturally enrich soils in Cr and Ni (Tassi et al., 2018), providing a plausible source of this signal. Conversely, the negative loading of Sb (−0.68) points to independent anthropogenic inputs, such as waste incineration and vehicular emissions (including brake and tyre wear; Yang et al., 2022), thereby highlighting that PC1 primarily contrasts natural (Cr–Ni–rich) versus anthropogenic (Sb-rich) signatures. PC2 (20.8 % of variance) reflected a natural-anthropogenic gradient. Positive loadings for As (0.41) and Zn (0.71) indicate legacy pyrite roasting and urban dust inputs, while negative loadings for Co (−0.81) and Mn (−0.67) suggest a natural geochemical background and soil resuspension. Nearby TiO_2 production facility emissions may also have contributed to this component. PC3 (14.0 % of variance) captured specialised industrial signatures, with strong positive Sn loading and negative Tl loading. Sn is typically associated with electronics manufacturing, waste disposal, and plating processes, whereas Tl is linked to waste incineration, sulfide ore smelting, and other industrial activities (Migaszewski and Gałuszka, 2021). PC4 (10.7 %) and PC5 (9.6 %) exhibited finer-scale variability. The elevated Cd loading in PC5 suggests episodic or localised emissions, potentially from fertiliser application or smelting operations.

Fig. 7 displays a biplot of the first two principal components (PC1 and PC2), which together explained 44.1 % of the total variance.

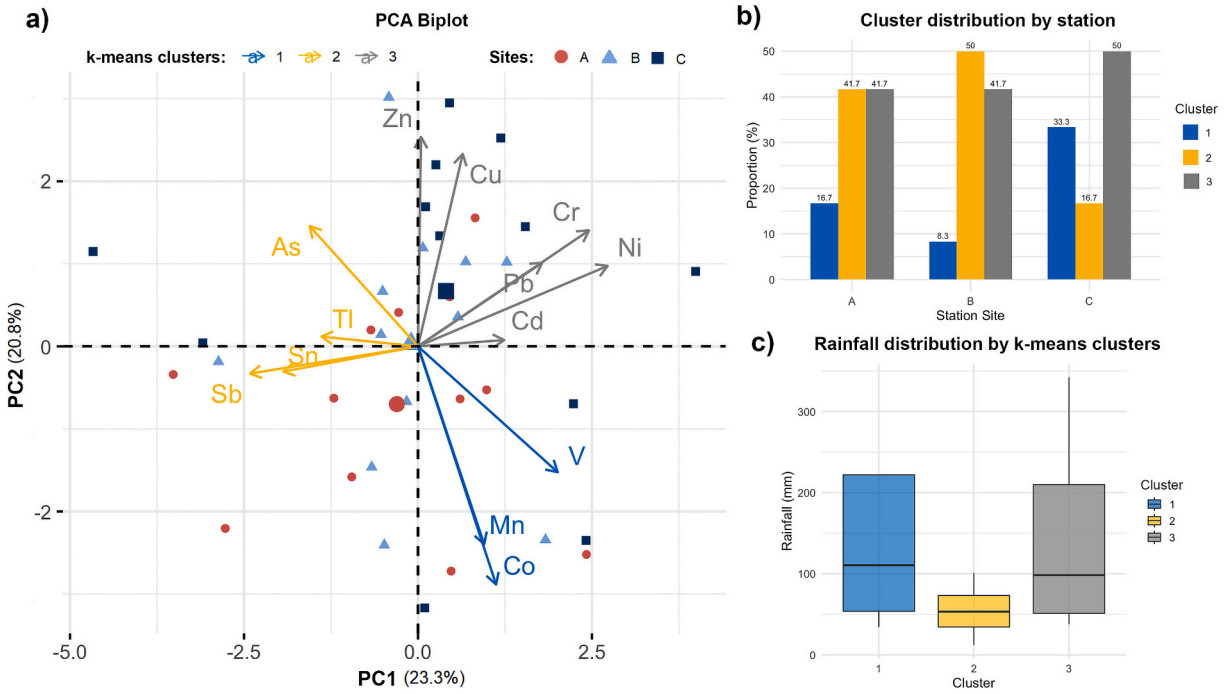

Fig. 7. PCA biplot (a) showing the first two components (PC1: 23.3 %, PC2: 20.8 %) based on PTEs in bulk deposition. Arrows denote the contribution and directionality of each element, with vector length reflecting relative influence on the principal components. Data points are colour-coded and shaped by sampling site. K-means clustering was applied to the PCA output, delineating distinct compositional groups among samples, as illustrated in panel (b). Panel (c) displays the rainfall distribution across k-means clusters, highlighting differences in precipitation regimes potentially influencing deposition profiles.

These components effectively captured the major dataset patterns, illustrating the spatial differences in PTE profiles and their contributions to bulk deposition trends. To enhance the interpretation of these multivariate patterns, k-means clustering grouped the sampling sites according to their elemental composition and depositional characteristics (Fig. 7b). ANOVA ($p < 0.05$) revealed significant rainfall differences among clusters (Fig. 7c), with Tukey's HSD post hoc tests indicating that Cluster 2 experienced significantly lower precipitation than Clusters 1 and 3. Cluster analysis delineated distinct depositional regimes, reflecting compositional and meteorological variability across the study area.

These patterns can be summarized as follows:

- Cluster 1 - Predominantly associated with Site C, characterised by elevated Mn, Co, and V concentrations, suggesting combined natural and industrial contributions, including emissions from a nearby TiO_2 production facility (Jabłoński and Tylutka, 2016). Wet deposition likely enhanced the flux of soluble elements, whereas less soluble components were transported via soil resuspension, consistent with Pan and Wang (2015).
- Cluster 2 - Linked primarily to Sites A and B, exhibiting elevated As and Sb levels reflecting strong anthropogenic influence compounded by local geochemical conditions. Historical and ongoing industrial activities have dominated, with dry deposition processes being critical under reduced precipitation conditions, as reported by Nie et al. (2017) for low-rainfall environments.

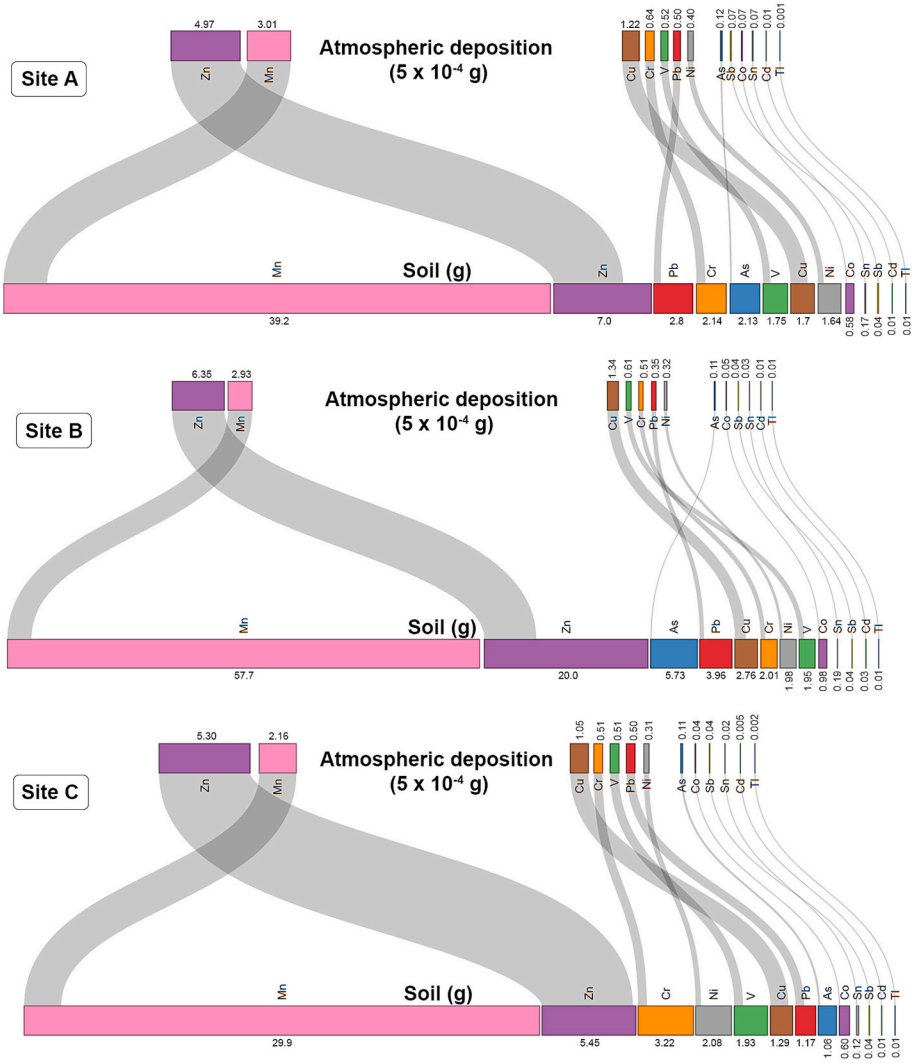

Fig. 8. Proportional flow diagram illustrating the annual contribution of potentially toxic elements (PTEs) from atmospheric bulk deposition to the total PTE mass in surface soils (0–5 cm depth) at Sites A, B, and C. Elements are ordered from left to right based on their quantities in atmospheric deposition and corresponding soil inventories. To facilitate visualisation, deposition fluxes were normalised to 5×10^{-4} g. Soil PTE stocks were calculated for a volume of 0.05 m^3 (equivalent to a 1 m^2 area and 5 cm depth), assuming a bulk density of 1500 kg m^{-3}. The shaded connectors between atmospheric and soil pools represent the relative contribution of contemporary annual deposition fluxes (365 days) to the existing soil burdens.

- Cluster 3 - Defined by high Cr and Ni concentrations, indicating a clear geogenic origin with minimal industrial influence. Natural lithogenic sources predominated, with wet deposition facilitating the transport of soluble particulate matter. These findings align with observations from geologically active regions (Camarero et al., 2017) and support the seasonal deposition patterns described by Fernández-Olmo et al. (2015) and Pan et al. (2021).

The integration of PCA and cluster analysis extended the insights provided by univariate and bivariate approaches, effectively disentangling the complex interactions among industrial legacy, meteorological variability, and natural geochemical background. This multivariate framework enabled the robust characterisation of the three sampling sites, each exhibiting distinct PTE deposition profiles shaped by different environmental and anthropogenic factors.

Site A exhibited a pronounced source signature that was strongly associated with localised industrial activities. Situated at the urban periphery, this site underscores the critical role of atmospheric transport in the dissemination of anthropogenic PTEs. The juxtaposition of industrial operations and residential areas positions this site as an important indicator of potential human exposure and its associated health implications.

In contrast, Site B demonstrated a transitional depositional pattern that was heavily influenced by arsenopyrite sources and residues from industrial processes. The adjacent railway, a major national transport axis, constitutes an additional source of atmospheric trace element deposition via brake and wheel-rail abrasion processes that release particulate metals (e.g., Mn, Cu, Cr, and Ni; Bukowiecki et al., 2007; Burkhardt et al., 2008). Dry deposition processes dominated at this site, reflecting its intermediate position between industrial hotspots and natural settings. Site C was predominantly governed by wet deposition, indicative of regional geogenic background contributions, and served as a baseline reference for the Scarlino Plain.

These findings collectively reveal the intricate deposition patterns characteristic of a historically impacted peri-urban landscape, influenced by the interplay between diverse emission sources and contrasting land-use types. The three-site network highlights the dynamic interactions between natural and anthropogenic factors and the pronounced spatial heterogeneity of PTE fallout in the region. This integrative approach enhances our understanding of how complex source contributions and environmental variables affect contaminant deposition patterns, emphasising their importance for risk assessment and environmental management strategies.

3.4. Assessment of contribution of legacy PTEs pollution vs current inputs

To differentiate historical contamination from ongoing atmospheric inputs, we compared the mass of PTEs in surface soils (0–5 cm depth) with the annual deposition flux measured at three atmospheric deposition monitoring sites (A, B, and C). Topsoil (0–5 cm) concentrations were obtained at each site from samples collected from three nearby points (< 200 m from the passive collector apparatus), as determined by Monaci and Baroni (2025). Based on these soil concentrations, we estimated the total PTE mass per square meter of surface soil to a depth of 5 cm (0.05 m^3), assuming a bulk density of 1500 kg m^{-3}. The results are presented in Table S4 (Supplementary Material), which reports both soil concentration and the corresponding atmospheric deposition loads. These data were used to calculate *soil-to-deposition* (*S/D*) ratios, providing a metric for assessing the relative influence of current atmospheric inputs and existing soil contamination. Elevated *S/D* ratios indicate that legacy contamination substantially exceeds recent deposition.

Fig. 8 presents proportional flow diagrams comparing the annual deposition fluxes of PTEs with the corresponding topsoil inventories ranked by total soil mass. The shaded bands visually link elements between the atmospheric and soil compartments, illustrating the fraction of the topsoil inventory that could theoretically be attributed to one year of deposition. Several elements (As, Mn, and Co) exhibited high *S/D* ratios across all three sampling sites (Table S4), indicating a minimal contribution from current atmospheric inputs relative to the existing soil burden. These elevated ratios reflect the persistent legacy of historical industrial emissions, particularly from pyrite roasting operations, which continue to dominate soil contamination profiles despite source cessation. Notably, Mn, the most abundant PTE in the topsoil at all sites, demonstrated only moderate atmospheric deposition fluxes, confirming the predominant influence of legacy contamination on contemporary inputs.

Understanding the interplay between legacy contamination and contemporary atmospheric inputs is essential for assessing the ecological and human health risks of PTEs in the Scarlino Plain. This is particularly relevant for As, which has accumulated in soils through historical industrial activities, transforming them into long-term repositories and potential secondary emission sources. Meharg and Meharg (2021) demonstrated the dual role of As as a persistent soil contaminant and active participant in atmospheric cycling through microbial biovolatilization and arsine emissions. They identified mineral soils and wetlands as significant As reservoirs, where climatic factors, such as elevated temperature and moisture, can enhance atmospheric release through increased volatilisation rates (Meharg and Meharg, 2021; Nie et al., 2017).

Zinc and Cu exhibited lower *S/D* ratios, indicating that while soil concentrations reflect historical contamination, ongoing emissions from traffic, light industry, and residual operations remain significant contributors. As demonstrated in Section 3.1, Zn shows elevated atmospheric deposition fluxes despite a lower total soil mass than Mn, highlighting the combined influence of legacy and contemporary sources on Zn accumulation. These data indicate that soil inventories of As, Mn, and Co are predominantly governed by historical contamination, whereas Zn and Cu reflect mixed signals with meaningful ongoing atmospheric contributions, albeit at lower levels.

Although deposition fluxes in the Scarlino Plain are substantially lower than those in heavily industrialised regions with active smelting operations (e.g. Qiu et al., 2016; Yu et al., 2022), they remain sufficient to influence long-term PTE cycling and their bioavailability in soil matrices. These findings align with previous research demonstrating that legacy contamination dominates the total soil concentrations in deindustrialised regions (Xing et al., 2020; Zhu et al., 2016). Following the closure or reduction of major point sources, historically contaminated soils continue to affect local environments through the resuspension of contaminated

particles. Furthermore, contemporary atmospheric inputs, although lower in magnitude, may enhance the mobility and bioavailability of legacy-bound elements under acidic or redox-variable conditions (Cui et al., 2024; Meharg and Meharg, 2021).

Despite regulatory measures and stricter emission controls that have substantially reduced the atmospheric deposition of Cd, Pb, and Zn over recent decades (Yu et al., 2022; Zhu et al., 2016), the corresponding reductions in total soil burdens remain limited. This persistence highlights the stability and long-term environmental significance of legacy contamination reservoirs (Pan et al., 2021; Yu et al., 2022).

The Scarlino Plain exemplifies this dual contamination scenario, with substantial historical industrial deposition coupled with ongoing contemporary inputs. Although current atmospheric deposition contributes proportionally less to total soil burdens, it continues to influence elemental speciation, metal mobility, and ecological risk. Therefore, effective remediation strategies must prioritise the stabilization of historically accumulated contaminants while maintaining surveillance and control of contemporary atmospheric sources.

4. Limitations

This study has four principal constraints. First, the single-year monitoring period (2014–2015) provides a temporally bounded snapshot that may not capture interannual variability in emissions and meteorology. Yet our design, monthly bulk (wet + dry) deposition at three sites for one year, is consistent with established practice, sitting between long single-site time series and broader regional networks that use bulk collectors to characterise spatial patterns and risks (Camarero et al., 2017; Pan et al., 2021; Ma et al., 2024; Liu et al., 2024; Brugnone et al., 2023; Fernández-Olmo et al., 2015). Second, limited spatial replication ($n = 3$) constrains fine-scale source discrimination and localised hotspot detection. While multivariate analysis partially mitigates this limitation, expanded site networks would improve source apportionment resolution. Third, the use of bulk passive collectors precludes separation of wet versus dry inputs, particle-size resolution, and operational chemical fractions (e.g., water-soluble vs particulate-bound), all of which influence deposition velocities, bioavailability, and pathway inference. Addressing these aspects requires parallel wet/dry sampling, size-fractionation, and fraction-specific analyses, which demonstrably sharpen risk and process attribution in recent assessments (Pan and Wang, 2015; Xia et al., 2024; Pan et al., 2021). Fourth, the fragmented European regulatory framework and absence of Italian-specific reference values for atmospheric metal deposition complicate risk interpretation. While TA-Luft guidelines and critical-load concepts provide comparative benchmarks, harmonised Mediterranean standards would strengthen policy relevance (Ianiri et al., 2024; Schlutow et al., 2021).

Future investigations should prioritise: *i*) multi-year monitoring to capture temporal variability; *ii*) denser spatial networks targeting emission corridors; *iii*) wet/dry separation with size-fractionation and speciation analyses; and *iv*) advanced source apportionment (PMF, isotopic tracers) integrated with ecological receptors, building on recent methodological advances (Pan et al., 2021; Ma et al., 2024).

5. Conclusions

This study provides a comprehensive assessment of PTE deposition across the Scarlino Plain, revealing how industrial legacy, local meteorology, and geogenic inputs interact to shape the distribution patterns of contaminants. Spatial deposition patterns reflect contributions from both wet and dry processes, demonstrating the combined influence of anthropogenic and natural background sources. The observed heterogeneity reveals the inherent complexity of PTE fluxes in peri-urban industrial environments.

Key findings demonstrate that major elements (Zn and Mn) exhibit relatively uniform deposition, indicating diffuse source contributions. Conversely, episodic enrichments of Sb, Sn, and Pb suggest localised industrial activities, emphasising the need for continued monitoring. Notably, recurrent As exceedances above peri-urban baseline thresholds present significant ecological and public health concerns that require further investigation.

From a management perspective, these results emphasise the necessity of integrated environmental strategies that address both legacy contamination and contemporary emissions. Effective mitigation requires complementary approaches: stabilization of historical contaminants coupled with stringent source controls to prevent ongoing soil and biota enrichment. Sustained atmospheric monitoring and adaptive regulatory frameworks are essential for preserving ecosystem integrity and minimising human exposure in this complex industrial landscape.

Funding

This study was partially funded by Scarlino Energia S.r.l. in the framework of an Environmental Impact Assessment (EIA) permitting procedure conducted under the EU Directive, authorized by the Province of Grosseto (Administrative Determination No. 2988, dated 24/10/2012).

CRediT authorship contribution statement

Fabrizio Monaci: Writing – review & editing, Writing – original draft, Visualization, Supervision, Funding acquisition, Formal analysis, Conceptualization. **Davide Baroni:** Writing – review & editing, Methodology, Investigation, Data curation, Conceptualization.

Declaration of competing interest

The authors declare the following financial interests/personal relationships which may be considered as potential competing interests: Fabrizio Monaci reports financial support was provided by Scarlino Energia Srl. If there are other authors, they declare that they have no known competing financial interests or personal relationships that could have appeared to influence the work reported in this paper.

Data availability

Data will be made available on request.

Acknowledgments

The authors thank the municipalities of Scarlino and Follonica for their support in granting permits and facilitating collaboration. We also appreciate the cooperation of private citizens who contributed to this project.

Fabrizio Monaci was supported under the National Recovery and Resilience Plan (NRRP), Mission 4 Component 2 Investment 1.4-Call for tender No. 3138 of 16 December 2021, rectified by Decree n.3175 of 18 December 2021 of Italian Ministry of University and Research funded by the European Union-NextGenerationEU; Award Number: Project code CN_00000033, Concession Decree No. 1034 of 17 June 2022 adopted by the Italian Ministry of University and *Re*-search, CUP B63C22000650007, Project title "National Biodiversity Future Center-NBFC".

Appendix A. Supplementary data

Supplementary data to this article can be found online at https://doi.org/10.1016/j.uclim.2025.102685.

References

Adhikari, S., Zeng, C., Zhang, F., Paudel Adhikari, N., Gao, J., Ahmed, N., Quaiyum Bhuiyan, M.A., Ahsan, M.A., Rahaman Khan, M.H., 2023. Atmospheric wet deposition of trace elements in Bangladesh: a new insight into spatiotemporal variability and source apportionment. Environ. Res. 217, 114729. https://doi.org/10.1016/j.envres.2022.114729.

Amato, F., Pandolfi, M., Moreno, T., Furger, M., Pey, J., Alastuey, A., Bukowiecki, N., Prevot, A.S.H., Baltensperger, U., Querol, X., 2011. Sources and variability of inhalable road dust particles in three European cities. Atmos. Environ. 45, 6777–6787. https://doi.org/10.1016/j.atmosenv.2011.06.003.

ARPAT, 2011. Monitoraggio della qualità dell'aria nella provincia di Grosseto. Comuni di Follonica e Scarlino. Rapporto relativo all'anno 2011.

ARPAT, 2014. Relazione sulla campagna di caratterizzazione di deposizioni umide e secche 2011–2013. In: Postazione Badia al Pino, comune di Civitella in Val di Chiana - Arezzo. Agenzia per la Protezione dell'Ambiente della Toscana, Florence.

Batonneau, Y., Bremard, C., Gengembre, L., Laureyns, J., Le Maguer, A., Le Maguer, D., Perdrix, E., Sobanska, S., 2004. Speciation of PM10 sources of airborne nonferrous metals within the 3-km zone of Lead/zinc smelters. Environ. Sci. Technol. 38, 5281–5289. https://doi.org/10.1021/es0497173.

Brugnone, F., D'Alessandro, W., Parello, F., Brusca, L., Saiano, F., Li Vigni, L., Sprovieri, M., Calabrese, S., 2023. Atmospheric deposition around the industrial areas of Milazzo and Priolo Gargallo (Sicily–Italy)—part B: trace elements. Atmosphere 14, 737. https://doi.org/10.3390/atmos14040737.

Bukowiecki, N., Gehrig, R., Hill, M., Lienemann, P., Zwicky, C.N., Buchmann, B., Weingartner, E., Baltensperger, U., 2007. Iron, manganese and copper emitted by cargo and passenger trains in Zürich (Switzerland): size-segregated mass concentrations in ambient air. Atmos. Environ. 41, 878–889. https://doi.org/10.1016/j.atmosenv.2006.07.045.

Burkhardt, M., Rossi, L., Boller, M., 2008. Diffuse release of environmental hazards by railways. Desalination 226, 106–113. https://doi.org/10.1016/j.desal.2007.02.102.

Camarero, L., Bacardit, M., De Diego, A., Arana, G., 2017. Decadal trends in atmospheric deposition in a high elevation station: effects of climate and pollution on the long-range flux of metals and trace elements over SW Europe. Atmos. Environ. 167, 542–552. https://doi.org/10.1016/j.atmosenv.2017.08.049.

Chen, Y., Wang, Q., Zhu, J., Xi, Y., Zhang, Q., Dai, G., He, N., Yu, G., 2022. Atmospheric wet Iron, molybdenum, and vanadium deposition in Chinese terrestrial ecosystems. Environ. Sci. Technol. 56, 12898–12905. https://doi.org/10.1021/acs.est.2c03213.

Comas-Cufí, M., Thió-Henestrosa, S., 2011. CoDaPack 2.0: A stand-alone, multi-platform compositional software. In: CoDaPack 2.0: A Stand-Alone, Multi-Platform Compositional Software. Sant Feliu de Guíxols, Spain.

Costagliola, P., Benvenuti, M.M., Benvenuti, M.G., Di Benedetto, F., Lattanzi, P., 2010. Quaternary sediment geochemistry as a proxy for toxic element source: a case study of arsenic in the Pecora Valley (southern Tuscany, Italy). Chem. Geol. 270, 80–89. https://doi.org/10.1016/j.chemgeo.2009.11.007.

Cui, H., Zhao, Y., Hu, K., Xia, R., Zhou, Jing, Zhou, Jun, 2024. Impacts of atmospheric deposition on the heavy metal mobilization and bioavailability in soils amended by lime. Sci. Total Environ. 914, 170082. https://doi.org/10.1016/j.scitotenv.2024.170082.

Feng, D., Gong, P., Li, Y., Li, N., Dong, Z., Zhu, Z., Jiang, R., Deng, S., 2023. Risk assessment and source apportionment of heavy metals pollution from atmospheric deposition in Nanjing, China. Heliyon 9, e18858. https://doi.org/10.1016/j.heliyon.2023.e18858.

Fernández-Olmo, I., Puente, M., Montecalvo, L., Irabien, A., 2014. Source contribution to the bulk atmospheric deposition of minor and trace elements in a northern Spanish coastal urban area. Atmos. Res. 145–146, 80–91. https://doi.org/10.1016/j.atmosres.2014.04.002.

Fernández-Olmo, I., Puente, M., Irabien, A., 2015. A comparative study between the fluxes of trace elements in bulk atmospheric deposition at industrial, urban, traffic, and rural sites. Environ. Sci. Pollut. Res. 22, 13427–13441. https://doi.org/10.1007/s11356-015-4562-z.

Fujiwara, F., Rebagliati, R.J., Marrero, J., Gómez, D., Smichowski, P., 2011. Antimony as a traffic-related element in size-fractionated road dust samples collected in Buenos Aires. Microchem. J. 97, 62–67. https://doi.org/10.1016/j.microc.2010.05.006.

Guo, L., Lyu, Y., Yang, Y., 2017. Concentrations and chemical forms of heavy metals in the bulk atmospheric deposition of Beijing, China. Environ. Sci. Pollut. Res. 24, 27356–27365. https://doi.org/10.1007/s11356-017-0324-4.

Ianiri, G., Settimo, G., Avino, P., 2024. Atmospheric bulk depositions: state-of-the-art and European legislative framework with focus on Italy. Environ. Sci. Pollut. Res. https://doi.org/10.1007/s11356-024-34338-y.

Jabłoński, M., Tylutka, S., 2016. The influence of initial concentration of sulfuric acid on the degree of leaching of the main elements of ilmenite raw materials. J. Therm. Anal. Calorim. 124, 355–361. https://doi.org/10.1007/s10973-015-5114-y.

Jiang, S., Dong, X., Han, Z., Zhao, J., Zhang, Y., 2024. Emissions and atmospheric dry and wet deposition of trace metals from natural and anthropogenic sources in mainland China. Atmosphere 15, 402. https://doi.org/10.3390/atmos15040402.
Lê, S., Josse, J., Husson, F., 2008. FactoMineR: an R package for multivariate analysis. J. Stat. Softw. 25, 1–18. https://doi.org/10.18637/jss.v025.i01.
Li, Y., Yuan, Y., Sun, C., Sun, T., Liu, X., Li, J., Fang, L., Fan, Z., 2020. Heavy metals in soil of an urban industrial zone in a metropolis: risk assessment and source apportionment. Stoch. Env. Res. Risk A. 34, 435–446. https://doi.org/10.1007/s00477-020-01779-z.
Liao, S., Jin, G., Khan, M.A., Zhu, Y., Duan, L., Luo, W., Jia, J., Zhong, B., Ma, J., Ye, Z., Liu, D., 2021. The quantitative source apportionment of heavy metals in peri-urban agricultural soils with UNMIX and input fluxes analysis. Environ. Technol. Innov. 21, 101232. https://doi.org/10.1016/j.eti.2020.101232.
Liu, P., Wu, Q., Hu, W., Tian, K., Huang, B., Zhao, Y., 2023. Effects of atmospheric deposition on heavy metals accumulation in agricultural soils: evidence from field monitoring and Pb isotope analysis. Environ. Pollut. 330, 121740. https://doi.org/10.1016/j.envpol.2023.121740.
Liu, Y., Gao, W., Chai, S., 2024. Assessment of fluxes and ecological and health risks of toxic trace elements in atmospheric deposition from the Baicheng-Songyuan area, Jilin Province Northeast China. Atmosphere 15, 744. https://doi.org/10.3390/atmos15070744.
Luft, T.A., 2002. First General Administrative Regulation Pertaining the Federal Immission Control act (Technical Instructions on Air Quality Control – TA Luft).
Ma, X., Sha, Z., Li, Y., Si, R., Tang, A., Fangmeier, A., Liu, X., 2024. Temporal-spatial characteristics and sources of heavy metals in bulk deposition across China. Sci. Total Environ. 926, 171903. https://doi.org/10.1016/j.scitotenv.2024.171903.
Månsson, N.S., Hjortenkrans, D.S.T., Bergbäck, B.G., Sörme, L., Häggerud, A.V., 2009. Sources of antimony in an urban area. Environ. Chem. 6, 160–169.
Meharg, A.A., Meharg, C., 2021. The pedosphere as a sink, source, and record of anthropogenic and natural arsenic atmospheric deposition. Environ. Sci. Technol. 55, 7757–7769. https://doi.org/10.1021/acs.est.1c00460.
Menichini, E., Barbera, S., Merli, F., Settimo, G., Viviano, G., 2006. Atmospheric bulk deposition of carcinogens PAHs in a rural area in southern Italy. Polycycl. Aromat. Compd. 26, 253–263. https://doi.org/10.1080/10406630600904026.
Migaszewski, Z.M., Gałuszka, A., 2021. Abundance and fate of thallium and its stable isotopes in the environment. Rev. Environ. Sci. Biotechnol. 20, 5–30. https://doi.org/10.1007/s11157-020-09564-8.
Monaci, F., Baroni, D., 2025. Spatial distribution and ecological risk of potentially toxic elements in peri-urban soils of a historically industrialised area. Environ. Monit. Assess. 197, 948. https://doi.org/10.1007/s10661-025-14389-5.
Morabito, E., Contini, D., Belosi, F., Stortini, A.M., Manodori, L., Gambaro, A., 2014. Atmospheric deposition of inorganic elements and organic compounds at the inlets of the Venice lagoon. Adv. Meteorol. 2014, 1–10. https://doi.org/10.1155/2014/158902.
Nie, X., Wang, Y., Li, Y., Sun, L., Li, T., Yang, M., Yang, X., Wang, W., 2017. Characteristics and impacts of trace elements in atmospheric deposition at a high-elevation site, southern China. Environ. Sci. Pollut. Res. 24, 22839–22851. https://doi.org/10.1007/s11356-017-8791-1.
Pan, Y.P., Wang, Y.S., 2015. Atmospheric wet and dry deposition of trace elements at 10 sites in northern China. Atmos. Chem. Phys. 15, 951–972. https://doi.org/10.5194/acp-15-951-2015.
Pan, Y., Liu, J., Zhang, L., Cao, J., Hu, J., Tian, S., Li, X., Xu, W., 2021. Bulk deposition and source apportionment of atmospheric heavy metals and metalloids in agricultural areas of rural Beijing during 2016–2020. Atmosphere 12, 283. https://doi.org/10.3390/atmos12020283.
Qiu, K., Xing, W., Scheckel, K.G., Cheng, Y., Zhao, Z., Ruan, X., Li, L., 2016. Temporal and seasonal variations of as, cd and Pb atmospheric deposition flux in the vicinity of lead smelters in Jiyuan, China. Atmos. Pollut. Res. 7, 170–179. https://doi.org/10.1016/j.apr.2015.09.003.
R Core Team, 2025. R: A Language and Environment for Statistical Computing. R Foundation for Statistical Computing, Vienna, Austria.
Rossato, L., Dughetti, F., Fontani, F., Paolieri, M., Tanelli, G., 2011. Arsenic and polymetallic anomalies in the Neogene-Quaternary sequence of La Botte borehole in the Scarlino Plain (Grosseto) Southern Tuscany Italy, njma 188, pp. 87–98. https://doi.org/10.1127/0077-7757/2011/0196.
Salminen, R., Batista, M.J., Bidovec, M., Demetriades, A., De Vivo, B., De Vos, W., Duris, M., Gilucis, A., Gregorauskiene, V., Halamic, J., Heitzmann, P., Lima, A., Jordan, G., Klaver, G., Klein, P., Lis, J., Locutura, J., Marsina, K., Mazreku, A., O'Connor, P.J., Olsson, S.Å., Ottesen, R.-T., Petersell, V., Plant, J.A., Reeder, S., Salpeteur, I., Sandström, H., Siewers, U., Steenfelt, A., Tarvainen, T., 2005. Geochemical Atlas of Europe. Part 1: Background Information, Methodology and Maps. Geological Survey of Finland, Espoo.
Savage, L., Carey, M., Williams, P.N., Meharg, A.A., 2019. Maritime deposition of organic and inorganic arsenic. Environ. Sci. Technol. 53, 7288–7295. https://doi.org/10.1021/acs.est.8b06335.
Schlutow, A., Schröder, W., Scheuschner, T., 2021. Assessing the relevance of atmospheric heavy metal deposition with regard to ecosystem integrity and human health in Germany. Environ. Sci. Eur. 33, 7. https://doi.org/10.1186/s12302-020-00391-w.
Tassi, E., Grifoni, M., Bardelli, F., Aquilanti, G., La Felice, S., Iadecola, A., Lattanzi, P., Petruzzelli, G., 2018. Evidence for the natural origins of anomalously high chromium levels in soils of the Cecina Valley (Italy). Environ Sci Process Impacts 20. https://doi.org/10.1039/C8EM00063H.
UNI, 2005a. UNI EN 14902:2005. Ambient air quality – Standard method for the measurement of Pb, Cd, As and Ni in the PM10 fraction of suspended particulate matter. Ente Nazionale Italiano di Unificazione (UNI), Milano.
UNI, 2005b. UNI CEI EN ISO/IEC 17025:2005. General Requirements for the Competence of Testing and Calibration Laboratories. Ente Nazionale Italiano di Unificazione (UNI), Milano.
Vandeuren, A., Pereira, B., Kaba, A.J., Titeux, H., Delmelle, P., 2023. Environmental bioavailability of arsenic, nickel and chromium in soils impacted by high geogenic and anthropogenic background contents. Sci. Total Environ. 902, 166073. https://doi.org/10.1016/j.scitotenv.2023.166073.
Vlasov, D., Kosheleva, N., Shinkareva, G., Kasimov, N., 2025. Contamination assessment and source identification of metals and metalloids in submicron road dust (PM1) in Moscow megacity. Environ. Sci. Pollut. Res. 32, 2085–2106. https://doi.org/10.1007/s11356-024-35791-5.
Wickham, H., 2016. ggplot2: Elegant Graphics for Data Analysis. Springer-Verlag, New York.
Wickham, H., François, R., Henry, L., Müller, K., 2023. Dplyr: a grammar of data manipulation. In: R package version 1.1.3.
Xia, R., Zhou, Jun, Mi, Y., Cui, H., Liu, H., Hu, K., Zhou, Jing, 2024. Chemical fractions of trace metals in atmospheric wet and dry deposition and contribution to rice root and foliar uptake. Plant Soil 494, 285–299. https://doi.org/10.1007/s11104-023-06274-2.
Xing, W., Yang, H., Ippolito, J.A., Zhao, Q., Zhang, Y., Scheckel, K.G., Li, L., 2020. Atmospheric deposition of arsenic, cadmium, copper, lead, and zinc near an operating and an abandoned lead smelter. J of Env Quality 49, 1667–1678. https://doi.org/10.1002/jeq2.20151.
Yang, C., Wu, Y., Zhang, L., Sun, G., Yao, H., Li, Z., Bi, X., Huang, Q., Feng, X., 2022. Spatiotemporal distributions and source apportionment of $PM_{2.5}$ -bound antimony in Beijing, China. JGR-Atmos. 127. https://doi.org/10.1029/2021JD036401 e2021JD036401.
Yao, C., Yang, Y., Li, C., Shen, Z., Li, J., Mei, N., Luo, C., Wang, Y., Zhang, C., Wang, D., 2024. Heavy metal pollution in agricultural soils from surrounding industries with low emissions: assessing contamination levels and sources. Sci. Total Environ. 917, 170610. https://doi.org/10.1016/j.scitotenv.2024.170610.
Yu, E., Liu, H., Tu, Y., Gu, X., Ran, X., Yu, Z., Wu, P., 2022. Superposition effects of zinc smelting atmospheric deposition on soil heavy metal pollution under geochemical anomaly. Front. Environ. Sci. 10, 777894. https://doi.org/10.3389/fenvs.2022.777894.
Yu, P., Han, Y., Wang, M., Zhu, Z., Tong, Z., Shao, X., Peng, J., Hamid, Y., Yang, X., Deng, Y., Huang, Y., 2023. Heavy metal content and health risk assessment of atmospheric particles in China: a meta-analysis. Sci. Total Environ. 867, 161556. https://doi.org/10.1016/j.scitotenv.2023.161556.
Yu, P., Shao, X., Wang, M., Zhu, Z., Tong, Z., Peng, J., Deng, Y., Huang, Y., 2024. Effects of atmospheric deposition on heavy metal contamination in paddy field systems under different functional areas in ChangZhuTan, Hunan Province, China. Sci. Total Environ. 933, 172953. https://doi.org/10.1016/j.scitotenv.2024.172953.
Zhang, Y., Zhang, S., Zhu, F., Wang, A., Dai, H., Cheng, S., Wang, J., Tang, L., 2018. Atmospheric heavy metal deposition in agro-ecosystems in China. Environ. Sci. Pollut. Res. 25, 5822–5831. https://doi.org/10.1007/s11356-017-0892-3.
Zhu, J., Wang, Q., Yu, H., Li, M., He, N., 2016. Heavy metal deposition through rainfall in Chinese natural terrestrial ecosystems: evidences from national-scale network monitoring. Chemosphere 164, 128–133. https://doi.org/10.1016/j.chemosphere.2016.08.105.